nature nanotechnology

LETTERS

PUBLISHED ONLINE: 26 JULY 2009 | DOI: 10.1038/NNANO.2009.193

Plasmonic fluorescent quantum dots

Yongdong Jin and Xiaohu Gao*

Combining multiple discrete components into a single multifunctional nanoparticle could be useful in a variety of applications. Retaining the unique optical and electrical properties of each component after nanoscale integration is, however, a long-standing problem[1,2]. It is particularly difficult when trying to combine fluorophores such as semiconductor quantum dots with plasmonic materials such as gold, because gold and other metals can quench the fluorescence[3,4]. So far, the combination of quantum dot fluorescence with plasmonically active gold has only been demonstrated on flat surfaces[5]. Here, we combine fluorescent and plasmonic activities in a single nanoparticle by controlling the spacing between a quantum dot core and an ultrathin gold shell with nanometre precision through layer-by-layer assembly. Our wet-chemistry approach provides a general route for the deposition of ultrathin gold layers onto virtually any discrete nanostructure or continuous surface, and should prove useful for multimodal bioimaging[6], interfacing with biological systems[7], reducing nanotoxicity[8], modulating electromagnetic fields[5] and contacting nanostructures[9,10].

Plasmonic engineering of nanomaterials has the potential to revolutionize a variety of research fields ranging from optoelectronics and nanophotonics to nanomedicine. For example, deposition of silver nanoparticles on thin-film solar cells has resulted in greater than tenfold enhancement in light absorption due to localized surface plasmons[11]. Similarly, when quantum dots (QDs) were spread on a rough gold film or a gold nanoparticle film, striking new spectral features including a fivefold increase in fluorescence intensity and 1,000 times faster excited-state lifetime were observed[5,12,13]. In the field of bioapplications, only fluorescence quenching has been explored so far, although pre-formed QDs and gold nanoparticles have been bridged with peptides for biosensing[4,14]. Despite these recent advances achieved on surfaces or based on nanoparticle clusters in solutions, a long-standing barrier has been how to functionalize single QDs with plasmonic materials such as gold while still maintaining the unique electronic and optical properties of both nanocomponents. Breakthrough work by Banin and colleagues shows selective growth of gold tips onto single-semiconductor QDs, quantum rods and tetrapods[1,2]. However, owing to the direct coupling of the gold and the semiconductor, the signature optical property of the semiconductor nanostructures, fluorescence, is nearly completely quenched in such arrangements. The key to solving this problem is to precisely tune the spacing between the gold and QDs and the plasmon band of the gold (for example, by coating the QDs with a gold shell of tunable thickness). Unfortunately, making discrete hybrid structures with tunable separation in the nanometre regime is extremely difficult, and current success remains on the theoretical analysis level[15].

Here, we report the development of gold-shell-encapsulated single QDs with well-defined gap and preserved optical properties. This homogeneous solution-based approach allows the formation of an ultrathin gold coating on both isolated nanostructures and continuous surfaces, and has direct relevance to problems frequently encountered in engineering sophisticated electronic devices and bioimaging probes, such as connecting molecules with electric sources in molecular electronics[9,10], producing multimodality imaging probes[6] and creating anchor points for simple biomolecule conjugation[7]. Furthermore, encapsulation of QDs made from toxic chemical elements (for example, CdSe)[8] with a thin layer of gold, which is biocompatible and highly stable[16,17], could potentially address concerns regarding QD toxicity, which is the determining factor for translational and clinical applications of QDs.

To encapsulate QDs with a gold shell and yet maintain their fluorescence, a number of problems must be addressed: (i) gold nanostructures are known fluorescence quenchers for both organic fluorophores and QDs[3,4]; (ii) a thick surrounding gold shell will block QD fluorescence transmittance[18]; (iii) the gold precursor, chloroauric acid ($HAuCl_4$), is highly acidic and corrosive, and can irreversibly damage QDs; (iv) the QD structural scaffold for gold shell growth is very small (a few nanometres); and (v) the space between the QD core and the gold shell must be precisely controlled. Previously, Halas and West have reported the preparation of gold nanoshells coated on large silica particles (120 nm) with shell thicknesses ranging from 5 to 20 nm (ref. 19). However, the core and shell 'touch' each other, which would completely quench fluorescence when the core is a QD[1,2]. In addition, these gold shells are too thick for efficient QD fluorescence transmission, and the thickness cannot be further reduced because the gold surface roughness is already 4 nm because of the large size of the gold nuclei[20].

Inspired by the biomineralization of gold[21], we solved the aforementioned problems using biomolecules as the structural scaffold (see Methods). The key is to first coat lipid-stabilized water-soluble QDs with a layer of peptide, poly-L-histidine (PLH), as the gold deposition template. In contrast to the commonly used primary amines[19,20], an important feature of PLH is that its histidine groups are capable of immobilizing Au^{3+} ions at very high packing density for deposition of thin and smooth gold shells (Fig. 1a). Binding between metals and histidine-containing peptides has been studied extensively because of their high affinities to metal ions. For example, the strong complexation between histidine-rich peptides and metals has been used for metallic nanotube synthesis[22], and is also one of the major mechanisms for protein purification[23]. For QD encapsulation, because $HAuCl_4$ is highly acidic, the pH value of the reaction solution was adjusted to 9–10 with NaOH to avoid QD damage. The separation between the QD core and the gold shell is determined by the size of the polyethylene glycol (PEG) chains and can be increased with nanometre precision by adding alternating polyelectrolyte monolayers such as polyallylamine hydrochloride (PAH, cationic) and sodium polystyrene sulphonate (PSS, anionic), a process also known as layer-by-layer (LBL) assembly (Fig. 1b)[5].

Figure 2 shows representative transmission electron microscopy (TEM) images of the QD–gold core–shell nanoparticles (Fig. 2c,d) and the original organic-soluble QDs (Fig. 2a) and water-soluble QDs (Fig. 2b) coated with lipids and PLH. Commercial QDs with

Department of Bioengineering, University of Washington, William H. Foege Building N530M, Seattle, Washington 98195, USA. *e-mail: xgao@u.washington.edu

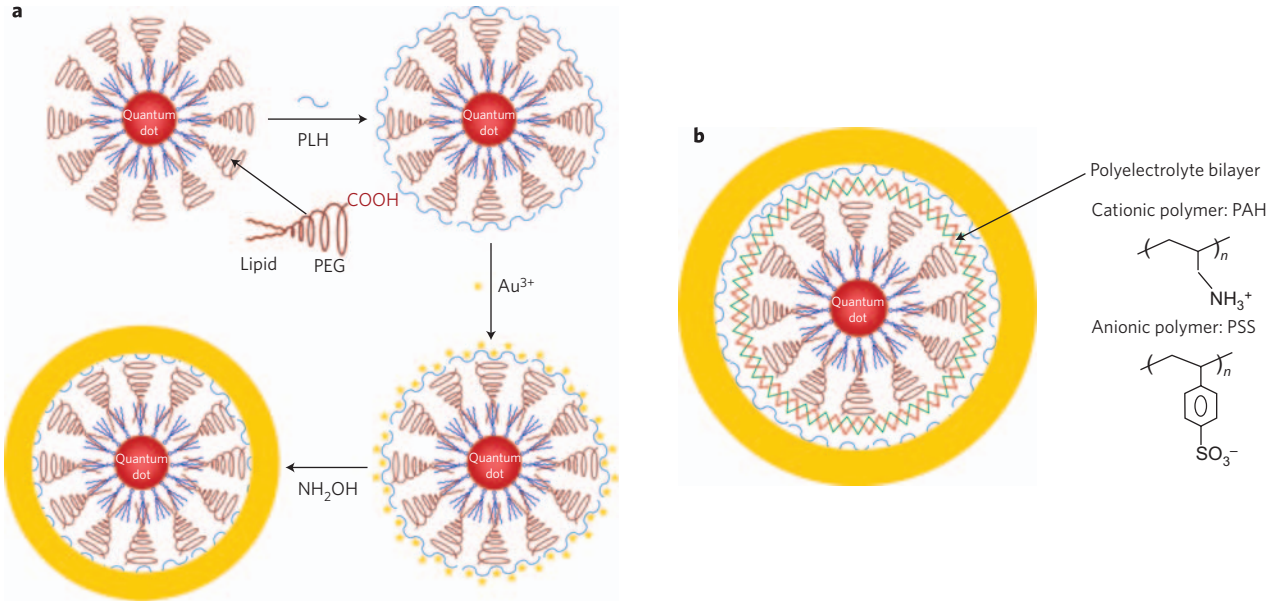

Figure 1 | Schematic of gold-shell-encapsulated quantum dots (QDs). a, Hydrophobic QDs coated with trioctylphosphine oxide (molecules on QD surface, blue) were solubilized with a lipid–PEG–COOH conjugate (purple). The water-soluble QDs were then coated with PLH (blue curves) for immobilization of Au^{3+} ions at high density. Addition of a mild reducing agent, hydroxylamine, led to gold nucleation on the PLH template and formation of a thin gold shell. **b**, The distance between the QD core and the gold shell can be precisely tuned by coating QDs with extra polyelectrolyte bilayers (cationic PAH and anionic PSS, red and green curves) by means of layer-by-layer (LBL) assembly before PLH coating. This figure is not drawn to scale.

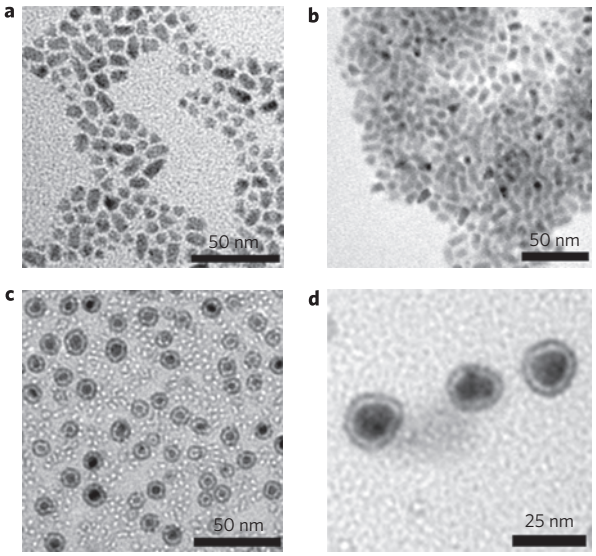

Figure 2 | TEM imaging of QD–gold hybrid nanoparticles. a–d, TEM images of QDs in chloroform (**a**), lipid–PEG–COOH conjugate-coated water-soluble QDs (**b**), gold-shell-encapsulated QDs shown at a magnification of 245,000 (**c**) and 340,000 (**d**). These TEM studies clearly show that virtually every QD is encapsulated by a thin gold shell (2–3 nm) with a gap between.

narrow emission peaks (full-width at half-maximum (FWHM), 32 nm) centred at 655 nm were used as the starting materials (Fig. 2a), which were insoluble in water. The lipid-based QD surface-coating method developed by Dubertret and colleagues was highly efficient in transferring QDs into aqueous solutions[24], yielding well dispersed particles (Fig. 2b). The soluble QDs remained single with successive adsorption of PLH and gold ions. After further gold deposition using a mild reducing reagent, hydroxylamine, the core–shell structure was clearly revealed by TEM (Fig. 2c,d). The shell thickness was ~2–3 nm, with a transparent gap of >3 nm observed between the core and shell because the sandwiched organic materials are not electron-dense enough for TEM visualization. This separation unambiguously shows that the gold deposition was not directly on the core particle surface[1], but was templated by the polymer outer layer. To the best of our knowledge, this TEM-based direct observation of well separated nanoparticle core–gold shell nanostructures has never been achieved.

Next, we thoroughly characterized the optical properties of the QD–gold nanoparticles. The QDs absorbed over a broad spectrum with increasing molar extinction coefficient towards shorter wavelengths and a first quantum confinement peak of 646 nm (Fig. 3a). After gold shell encapsulation, the QD absorption was buried under the strong gold surface plasmon resonance (SPR) peak centred at 583 nm. A key question was whether the encapsulated QDs would remain fluorescent, because gold nanostructures are known fluorescence quenchers and a gold shell will also limit photon transmittance. Quantitative spectroscopy measurements revealed that the original organic-soluble QDs and the lipid-coated water-soluble QDs shared a similar quantum yield (QY) of 75%, whereas that of the QD–gold nanoparticles decreased to 18% (Fig. 3c). Despite this fluorescence intensity decrease, the emission peak position did not shift. Detailed stepwise investigation of the synthesis revealed that the quenching occurred instantaneously upon the introduction of Au^{3+} ions, and this process accounted for approximately half of the total quenching effect. Although the exact mechanism is unclear at this time, likely a small number of Au^{3+} ions penetrated through the PEG layer and directly interacted with the QD surface. Several lines of evidence support this observation. First, the quenching effect was also observed for the control experiment without the PLH coating layer, indicating that the quenching was not due to the Au^{3+} ions adsorbed on the polymer. Second, for QDs solubilized with small-molecule mercapto compounds, the fluorescence was completely quenched due to the higher accessibility of Au^{3+} to the QD surface. In addition, a similar effect has been observed previously with Ag^+, Pb^{2+} and Cu^{2+} ions and has been attributed to cation exchange in the nanocrystals' lattice[25].

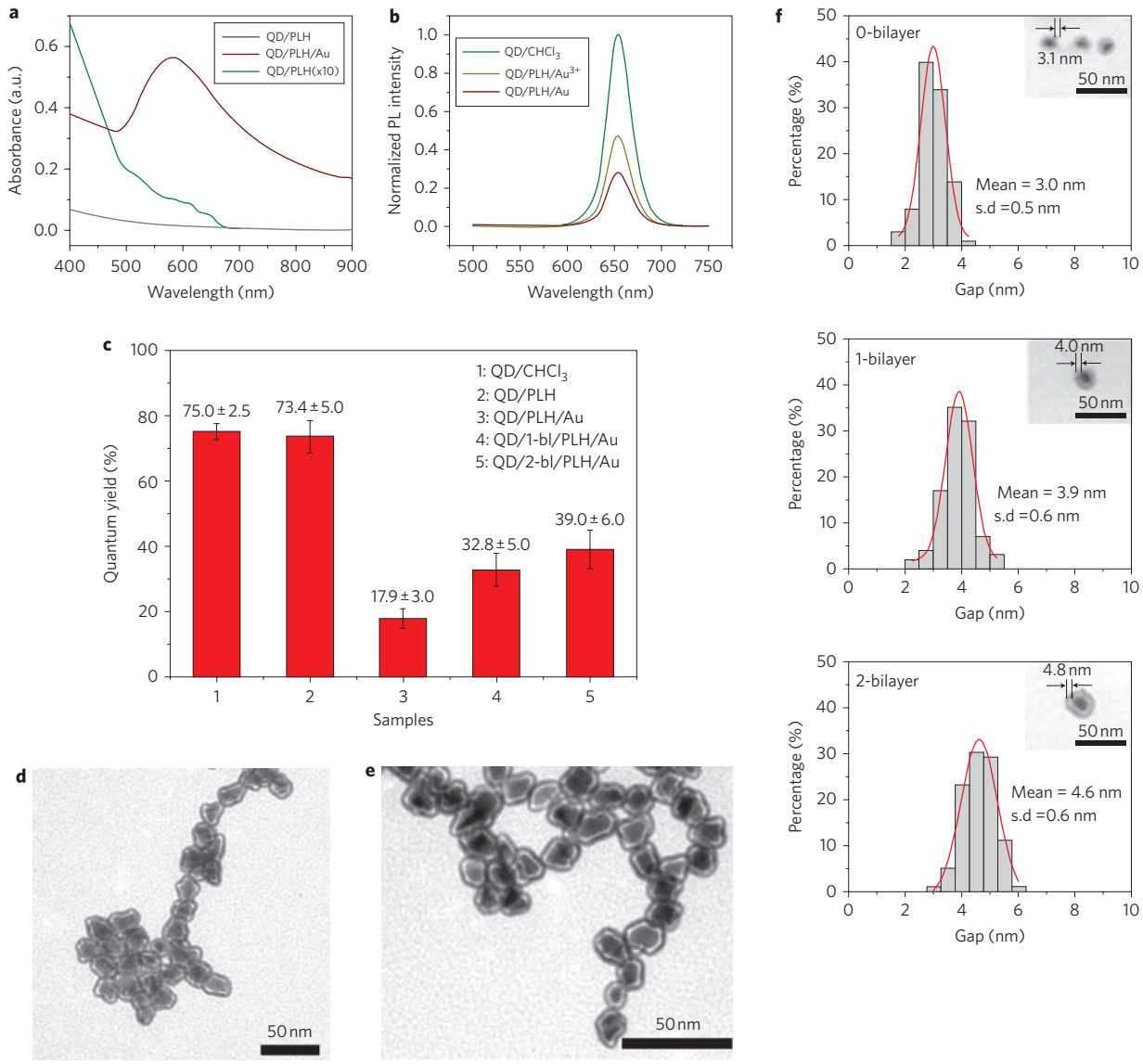

Figure 3 | Optical properties of the QD–gold core–shell nanoparticles. a, UV-vis absorption of the QDs before and after gold encapsulation. The black (original) and green (absorption value ×10 for better visualization) curves show the absorption profile of the water-soluble PLH-coated QD. After gold shell formation, the QD absorption was buried by a strong surface plasmon resonance (SPR) band centred at 583 nm. **b**, Fluorescence spectra of the original organic-soluble QDs (green), water-soluble QDs in the presence of Au^{3+} ions (yellow), and gold-shell-encapsulated QDs (red). Although the peak position did not change, the fluorescence intensity decreased 51.9% upon addition of Au^{3+} salt, and decreased another 23.7% after gold shell formation. **c**, To improve the QD fluorescence efficiency, polyelectrolyte bilayers composed of cationic PAH and anionic PSS were deposited onto the QD surface before PLH coating to increase the spacing between the QD core and the gold shell. Quantitative spectroscopic measurements indicated that the QD fluorescence was significantly improved with one to two layers of polyelectrolyte coating. The final QD quantum yield increased to 32.8% with one layer of PAH/PSS and 39.0% with two layers of PAH/PSS. **d**,**e**, Representative TEM images of the QD–gold core–shell nanoparticles with one and two layers of polyelectrolyte spacers. **f**, Histograms of the core–shell separation distribution of particles with zero bilayers (top), one bilayer (middle) and two bilayers (bottom) of polyelectrolytes. Each histogram was plotted based on >100 nanoparticles. Insets show the TEM measurements of representative particles.

The second factor that could affect the fluorescence is the thickness of the gold shell. The thicker the shell, the more fluorescence will be blocked. Based on our peptide templated gold deposition, we were able to achieve a 2–3 nm thin gold layer. Under the current experiment conditions (excitation 400 nm and emission 655 nm), the light transmittance values for excitation and emission were 86% and 92% through the thin gold shell, collectively resulting in ~20% fluorescence attenuation[18]. The QD fluorescence decreased gradually with slight increase of the gold shell thickness and was significantly quenched when this was greater than 5 nm. The third major factor that affects the QD fluorescence is the gold shell SPR, which can simultaneously quench and enhance the QD fluorescence (competing processes) depending on the spacing between the two materials and the spectral overlap between the QD fluorescence and the gold SPR. At short separation distance and significant overlap between QD emission and gold SPR bands, the quenching effect dominates, whereas long distance and spectral overlap of QD absorption and gold SPR result in more pronounced field enhancement. Using gold nanoparticle films on a glass surface, Artemyet and colleagues show that by adjusting the QD and gold nanoparticle separation with polyelectrolytes, the QD fluorescence could be enhanced by a factor of up to five[5].

To optimize the QD–gold nanoparticle synthesis for improved fluorescence, we increased the QD core and gold shell separation

with successive adsorption of cationic and anionic polymers by means of LBL assembly, which is capable of reducing Au^{3+} diffusion to the QD surface and tuning the distance between the QD and gold with nanometre precision[5]. Unlike on flat surfaces, however, LBL on nanometre-sized particles requires multiple rounds of centrifuge-based purification for every layer of polyelectrolyte deposition (current experiments use three rounds for every polymer coating layer), which consequently results in an overall low QD recovery. Because of this limitation, we were only able to test two bilayers of polyelectrolyte coating (12 rounds of centrifugation in total). From the TEM images, small but statistically meaningful increments of the gap between the two electron-dense materials were measured. Figure 3f shows the histograms of the gap distribution obtained from more than 100 particles with zero, one and two bilayers. The average separations are 3.0 ± 0.5, 3.9 ± 0.6 and 4.6 ± 0.6 nm, respectively, which are smaller than the previously reported PAH/PSS bilayer thickness (~1.2 nm)[26] and could originate from the limited TEM image resolution and slight gold shell infiltration into the polyelectrolyte bilayers. Nevertheless, reproducible and quantitative fluorescence spectroscopy shows that the QD quantum yield increased to 33% with one additional bilayer of polyelectrolyte coating and 39% for two bilayers. We envision that future detailed studies on the effects of a broader range of core–shell spacing, shell thickness, and the overlap between the QD absorption and gold shell SPR bands, particularly in conjunction with theoretic modelling, could result in even brighter QDs. Although LBL assembly of PAH on flat surfaces could achieve 20 bilayers[5], LBL assembly on nanoparticles in solution for more than 2–3 layers is very difficult due to particle loss during repeated centrifugation. Other techniques such as encapsulating QDs with large amphiphilic block copolymers[27] could potentially solve this problem and allow effective and precise tuning (by changing polymer molecular weight) of the core–shell spacing over a larger range for detailed study of the separation-dependent fluorescence.

As well as the preserved QD fluorescence, two additional striking features were observed for the QD–gold core–shell nanoparticles. First, although QDs are known for their stability against photobleaching, the gold-encapsulated QDs exhibited significantly improved photostability over the lipid-stabilized water-soluble QDs, and even outperformed the original organic-soluble QDs under identical illumination conditions (Fig. 4a). This surprising feature is likely due to limited diffusion of oxygen through the gold shell because QD photobleaching is mainly caused by surface oxidation. Second, the strong scattering property of the gold shell renders the QD–gold an excellent dual-modality imaging probe. As shown in Figure 4b–g, samples of dilute uncoated and gold-shell-encapsulated QDs were spread on glass coverslips, resulting in spatially isolated single nanoparticles on the surface. Fluorescence and dark-field imaging show that the uncoated QDs were fluorescent but not plasmonic. In contrast, the QD–gold nanoparticles in the fluorescence and dark-field imaging micrographs show nearly complete overlap, which also confirms the successful encapsulation of QDs with thin gold shells. It is widely known that each type of nanoprobe has distinct advantages as well as limitations. This new class of multimodality nanoprobe will allow imaging with both fluorescence and scattering as well as light-triggered photothermal treatment (particularly when the surface plasmon band is tuned to the NIR region). These modes of imaging and therapy cannot be achieved simultaneously with the traditional small molecule-, amphiphilic polymer- and silica-coated QDs. Other important advantages over the traditional QDs could also be expected, such as potentially simplified bioconjugation due to the well-established thiolate–gold chemistry and improved biocompatibility.

In conclusion, the first successful preparation of gold-shell-encapsulated QDs by means of peptide-templated shell growth has been achieved. Although gold nanoparticles have been demonstrated as efficient fluorescence quenchers, we found that precise control of the spacing between the QD core and the gold shell resulted in QDs with a quantum yield of 39%, and this value could be further improved by optimizing parameters such as a broader range of core–shell spacing, shell thickness, and overlap between the QD fluorescence and gold-shell SPR bands. The thin gold shell also shows strong surface plasmon scattering, which makes the QD–gold nanoparticles an excellent dual-modality imaging probe. In addition, because recently reported monodisperse

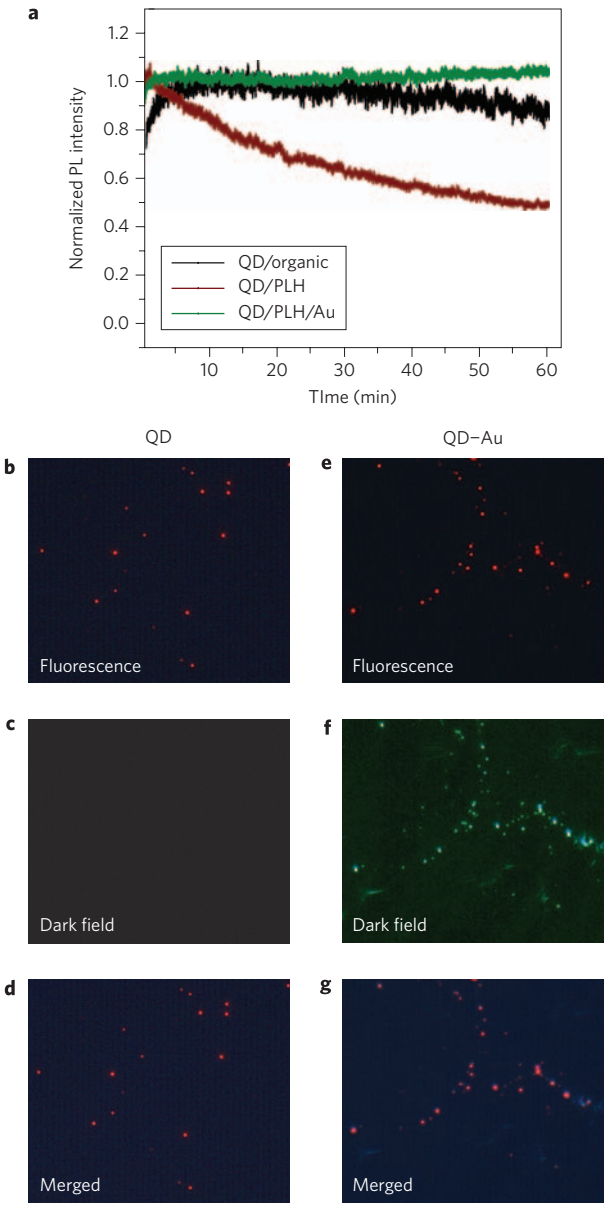

Figure 4 | Photostability and dual imaging modalities of the QD–gold nanonanoparticles. a, Normalized fluorescence intensities of organic soluble QDs, water-soluble QDs and gold-coated QDs. Under identical illumination conditions (480/40 nm), the QD–gold nanoparticles are significantly more photostable than the lipid-PEG-coated water-soluble QDs, and even slightly outperformed the original organic-soluble QDs. **b–g**, Fluorescence and dark-field imaging of single nanoparticles spread between two glass coverslips. For QDs without gold shell coating (**b–d**), only fluorescence signals were observed, but no scattering signal. In contrast, because of the metallic gold shell, the encapsulated QDs (**e–g**) not only exhibited strong fluorescence, but also became excellent probes for surface plasmon scattering.

nanostructures often have a similar surface chemistry as QDs (for example, monolayer of hydrophobic ligands)[28], this technology can serve as a general route for encapsulating a variety of discrete nanomaterials and modulating their surrounding electromagnetic field. We also envision that the degradation rate of the gold shell under physiological conditions will be significantly lower than those of small-molecule, silica and amphiphilic polymer coating layers[29,30], and thus prevent toxic chemicals from being released into the biological environment. This improved stability represents a potential solution to converting toxic nanomaterials into biocompatible materials, a critical step towards translational nanotechnology.

Methods

Unless specified, chemicals were purchased from Sigma-Aldrich and used without further purification. Organic soluble CdSe/ZnS QDs (Qdot 655 ITK) were purchased from Invitrogen. Lipid–PEG–COOH (DSPE–PEG_{2000} carboxylic acid) was purchased from Avanti Polar Lipids. Poly(allylamine hydrochloride) (M_{w3}, 15,000) and polystyrene sulphonate (Na salt) (M_w, 8,000, Polysciences) were used for the LBL polyelectrolyte deposition. Poly-L-histidine hydrochloride ($M_w \geq 5{,}000$) was used as the template to direct gold nucleation and growth. A UV-2450 spectrophotometer (Shimadzu) and a Fluoromax4 fluorometer (Horiba Jobin Yvon) were used to characterize the absorption and emission spectra of QDs. A table-top ultracentrifuge (Beckman TL120) was used for nanoparticle purification and isolation. The particle size was measured on a CM100 transmission electron microscope (Philips EO). HRTEM analysis was performed on a FEI TECNAI G2 F20 S-TWIN electron microscope. Fluorescence and dark-field images were obtained with an IX-71 inverted microscope (Olympus) and a Q-color5 digital colour camera (Olympus). For fluorescence imaging, broadband excitation in the blue range (460–500 nm) was provided by a mercury lamp. A long-pass dichroic filter (505 nm) and emission filter (510 nm, Chroma Technologies) were used to reject the scattered light and to pass the Stokes-shifted fluorescence signals.

Organic-soluble QD_{655} nanoparticles (1 μM solution in decane, 100 μl) were first flocculated by using a 4× methanol/isopropanol mixture (v/v 75/25), and resuspended in chloroform (1 ml). Lipid–PEG–COOH (3 mg) was added to the solution and sonicated for 5 min followed by removal of the chloroform by evaporation. The residual solid was heated to 80 °C for 5 min, followed by addition of deionized (DI) water (1 ml). Excess lipids were purified out from the solubilized QDs using repeated ultracentrifugation (30,000 rpm for 1 h, 3 times). The purified nanoparticles were redispersed in DI water (3 ml), to which PLH (1.5 mg) was added. The QDs and PLH were incubated at room temperature for ~1 h to allow PLH to adsorb onto the QD surface by electrostatic interaction. Excess PLH molecules were again removed by ultracentrifugation. The purified QD-PLH with a final concentration of 5.2 nM was dispersed in DI water and stored for use.

For gold shell growth, 890 μl of DI water and 10 μl of $HAuCl_4$ (w/w 1%) aqueous solution (pH adjusted to 9–10 with NaOH) were added to 100 μl of the QD–PLH, and incubated for ~10 min. A reducing agent NH_2OH (20 mM, 20 μl) was then introduced to initiate the surface-confined gold shell growth. Upon mixing, the colloidal solution changed from colourless to brownish blue over a few minutes, indicating formation of gold nanoshells. After synthesis, PEG–SH can be used to enhance the colloidal stability.

To adjust the QD core and gold shell separation, PAH and PSS stock solutions (10 mg ml^{-1} in 1 mM NaCl solution) were used for the LBL polyelectrolyte deposition onto the lipid–PEG-coated QDs before deposition of PLH and gold. In a typical preparation, 0.5 ml of PAH solution was added and mixed with 3 ml of the above synthesized water-soluble QDs suspended in 1 mM NaCl. After 30 min incubation, unbound PAH was removed by ultracentrifugation (three rounds). The same procedure was repeated for additional layers of polyelectrolytes and finally capped with a layer of PLH for gold nucleation and growth.

The QD quantum yield (QY) was determined relative to rhodamine 101, as its QY is well documented. During each step of polyelectrolyte coating, the QY of the QD–polymer complex can be easily determined in the same manner. However, after gold shell formation on the surface of the QDs, the QD first extinction peak was buried by the strong gold plasmon peak, and as a consequence the QD concentration can no longer be determined using UV absorbance. Fortunately, due to the high reaction yield, virtually all QDs are encapsulated with a gold shell (confirmed with many randomly selected TEM images). Because the concentration of QDs before and after gold shell formation remained the same, the QY values of QD–gold can be calculated using QD–PLH as a reference in fluorescence spectroscopy measurements.

Given that TEM imaging under inappropriate focusing conditions can sometimes show blurred ring structures around nanoparticles, HRTEM was performed to ensure that the core–shell structure observed was not an imaging artifact (see Supplementary Fig. S1). At a magnification of 1.05 M, the crystal lattices of the semiconductor core and the gold shell became visible. Owing to the low contrast of HRTEM on ultrathin nanomaterials[31], the image contrast in Supplementary Fig. S1a was not as high as the low-magnification images in Fig. 2, and some areas appeared to be gaps. However, enlarged imaging (see Supplementary Fig. S1b) at the 'gap' area clearly showed the signature lattice fringe of gold, confirming the existence of a thin gold shell. A similar contrast drop under HRTEM has also been observed on ultrathin (~2 nm) gold nanowires when the nanowire thickness was reduced only slightly[32,33]. The HRTEM images also revealed the polycrystalline property of the gold nanoshell, which was not apparent when examined at low magnifications.

Received 5 May 2009; accepted 24 June 2009;
published online 26 July 2009

References

1. Mokari, T., Rothenberg, E., Popov, I., Costi, R. & Banin, U. Selective growth of metal tips onto semiconductor quantum rods and tetrapods. *Science* **304,** 1787–1790 (2004).
2. Mokari, T., Sztrum, C. G., Salant, A., Rabani, E. & Banin, U. Formation of asymmetric one-sided metal-tipped semiconductor nanocrystal dots and rods. *Nature Mater.* **4,** 855–863 (2005).
3. Dubertret, B., Calame, M. & Libchaber, A. J. Single-mismatch detection using gold-quenched fluorescent oligonucleotides. *Nature Biotechnol.* **19,** 365–370 (2001).
4. Pons, T. *et al.* On the quenching of semiconductor quantum dot photoluminescence by proximal gold nanoparticles. *Nano Lett.* **7,** 3157–3164 (2007).
5. Kulakovich, O. *et al.* Enhanced luminescence of CdSe quantum dots on gold colloids. *Nano Lett.* **2,** 1449–1452 (2002).
6. Cai, W. B. & Chen, X. Y. Nanoplatforms for targeted molecular imaging in living subjects. *Small* **3,** 1840–1854 (2007).
7. Elghanian, R., Storhoff, J. J., Mucic, R. C., Letsinger, R. L. & Mirkin, C. A. Selective colorimetric detection of polynucleotides based on the distance-dependent optical properties of gold nanoparticles. *Science* **277,** 1078–1081 (1997).
8. Derfus, A. M., Chan, W. C. W. & Bhatia, S. N. Probing the cytotoxicity of semiconductor quantum dots. *Nano Lett.* **4,** 11–18 (2004).
9. Haick, H. & Cahen, D. Contacting organic molecules by soft methods: towards molecule-based electronic devices. *Acc. Chem. Res.* **41,** 359–366 (2008).
10. Hipps, K. W. Molecular electronics: It's all about contacts. *Science* **294,** 536–537 (2001).
11. Pillai, S., Catchpole, K. R., Trupke, T. & Green, M. A. Surface plasmon enhanced silicon solar cells. *J. Appl. Phys.* **101,** 093105 (2007).
12. Shimizu, K. T., Woo, W. K., Fisher, B. R., Eisler, H. J. & Bawendi, M. G. Surface-enhanced emission from single semiconductor nanocrystals. *Phys. Rev. Lett.* **89,** 117401 (2002).
13. Pompa, P. P. *et al.* Metal-enhanced fluorescence of colloidal nanocrystals with nanoscale control. *Nature Nanotech.* **1,** 126–130 (2006).
14. Chang, E. *et al.* Protease-activated quantum dot probes. *Biochem. Biophys. Res. Commun.* **334,** 1317–1321 (2005).
15. Baer, R., Neuhauser, D. & Weiss, S. Enhanced absorption induced by a metallic nanoshell. *Nano Lett.* **4,** 85–88 (2004).
16. Jain, P. K., El-Sayed, I. H. & El-Sayed, M. A. Au nanoparticles target cancer. *Nano Today* **2,** 18–29 (2007).
17. Murphy, C. J. *et al.* Gold nanoparticles in biology: beyond toxicity to cellular imaging. *Acc. Chem. Res.* **41,** 1721–1730 (2008).
18. Liao, S. Y. Light transmittance and RF shielding effectiveness of a gold film on a glass substrate. *IEEE Trans. Electromagn. Compat.* **EMC-17,** 211–216 (1975).
19. Hirsch, L. R. *et al.* Metal nanoshells. *Ann.Biomed. Eng.* **34,** 15–22 (2006).
20. Oldenburg, S. J., Averitt, R. D., Westcott, S. L. & Halas, N. J. Nanoengineering of optical resonances. *Chem. Phys. Lett.* **288,** 243–247 (1998).
21. Reith, F., Rogers, S. L., McPhail, D. C. & Webb, D. Biomineralization of gold: biofilms on bacterioform gold. *Science* **313,** 233–236 (2006).
22. Djalali, R., Chen, Y.-F. & Matsui, H. Au nanocrystal growth on nanotubes controlled by conformations and charges of sequenced peptide templates. *J. Am. Chem. Soc.* **125,** 5873–5879 (2003).
23. Janknecht, R. *et al.* Rapid and efficient purification of native histidine-tagged protein expressed by recombinant vaccinia virus. *Proc. Natl Acad. Sci. USA* **88,** 8972–8976 (1991).
24. Dubertret, B. *et al. In vivo* imaging of quantum dots encapsulated in phospholipid micelles. *Science* **298,** 1759–1762 (2002).
25. Son, D. H., Hughes, S. M., Yin, Y. & Alivisatos, A. P. Cation exchange reactions in ionic nanocrystals. *Science* **306,** 1009–1012 (2004).
26. Caruso, F. Nanoengineering of particle surfaces. *Adv. Mater.* **13,** 11–22 (2001).
27. Chen, H. Y. *et al.* Encapsulation of single small gold nanoparticles by diblock copolymers. *ChemPhysChem* **9,** 388–392 (2008).
28. Park, J., Joo, J., Kwon, S. G., Jang, Y. & Hyeon, T. Synthesis of monodisperse spherical nanocrystals. *Angew Chem. Int. Ed.* **46,** 4630–4660 (2007).
29. Medintz, I. L., Uyeda, H. T., Goldman, E. R. & Mattoussi, H. Quantum dot bioconjugates for imaging, labelling and sensing. *Nature Mater.* **4,** 435–446 (2005).
30. Michalet, X. *et al.* Quantum dots for live cells, *in vivo* imaging and diagnostics. *Science* **307,** 538–544 (2005).

31. Wang, Z. L. Transmission electron microscopy of shape-controlled nanocrystals and their assemblies. *J. Phys. Chem. B* **104,** 1153–1175 (2000).
32. Lu, X., Yavuz, M. S., Tuan, H.-Y., Korgel, B. A. & Xia, Y. Ultrathin gold nanowires can be obtained by reducing polymeric strands of oleylamine–AuCl complexes formed via aurophilic interaction. *J. Am. Chem. Soc.* **130,** 8900–8901 (2008).
33. Wang, C. & Sun, S. H. Facile synthesis of ultrathin and single-crystalline Au nanowires. *Chem.-Asian J.* **4,** 1028–1034 (2009).

Acknowledgements

This work was supported in part by NIH (R01 CA131797, NSF, 0645080), the Seattle Foundation and the Department of Bioengineering at the University of Washington. X.G. thanks the NSF for a Faculty Early Career Development award (CAREER). We are especially grateful to T. Kavanagh and D. Eaton for fruitful discussions on nanotoxicity, UW Nanotech User Facility for HRTEM, Z. Wang and Y. Ding for TEM image interpretation, D. Chiu and D. Ginger for critical reading of the manuscript and D. Zhang for help with computer graphics.

Author contributions

Y.J. and X.G. conceived and designed the experiments. Y.J. performed the experiments. Y.J. and X.G. analysed and discussed the data. X.G. wrote the paper.

Additional information

Supplementary information accompanies this paper at www.nature.com/naturenanotechnology. Reprints and permission information is available online at http://npg.nature.com/reprintsandpermissions/. Correspondence and requests for materials should be addressed to X.G.